Time-Resolved FTIR Spectroscopy on Structure and Mobility of Single Crystal Ferroelectric Liquid Crystalline Elastomers

H. Skupin,*,† F. Kremer,† S. V. Shilov,†,‡ P. Stein,§ and H. Finkelmann§

Department of Physics and Geosciences, University of Leipzig, Linnéstr. 5, 04103 Leipzig, Germany; Inst. Macromolecular Compounds, Bolshoi pr. 31, 199004 St. Petersburg, Russia; and University of Freiburg, Inst. Macromolecular Chemistry, Sonnenstr. 5, 79104 Freiburg, Germany

Received August 28, 1998; Revised Manuscript Received February 11, 1999

ABSTRACT: Time-resolved polarized Fourier transform infrared (FTIR) spectroscopy on thin microtomized sections of single-crystal ferroelectric liquid crystalline elastomers (SC-FLCE) is employed to analyze its structure and mobility in response to an external electric field. Due to its specificity, FTIR spectroscopy enables to determine the orientation, the order parameter, and the extension and time scale of the motion for different molecular moieties. It is shown that under the influence of an external electric field the mesogenic units perform a motion on the tilt cone which is hindered by the elastomeric network. Although the different molecular moieties have a widely varying excursion of their motion, their response to the external electric field takes place simultaneously on a time scale of about 10 ms.

1. Introduction

Ferroelectric liquid crystalline elastomers (FLCE) are synthesized by the cross-linking of oriented FLC polymers or monomers.[1−5] By that one attains not only an improvement of the mechanical properties (rubber elasticity) but also a stabilization of the orientation of the mesogenic groups. The combination of ferroelectricity and rubber elasticity and the possibility to produce thin films of some nanometers thickness[1,21] makes FLCE a promising material for electromechanical applications in microsystem technology. To understand the molecular origin and the features of the electromechanical effect in FLCE,[6,7] it is necessary to analyze the molecular structure and mobility of these materials under the influence of an external electric field. For that time-resolved FTIR spectroscopy with polarized light is a powerful method. Although it was successfully used for the investigation of nonpolymeric and polymeric ferroelectrics,[9−17] data on elastomeric systems are still sparse.

2. Experimental Section

2.1. Sample Preparation. The investigated substance is a mechanically oriented single-crystal ferroelectric liquid crystalline elastomer (SC-FLCE, chemical structure shown in Figure 1). It consists of two different mesogenic parts and a polysiloxane backbone. The elastic network is formed by thermal cross-linking of polysiloxane chains lying preferably in adjacent smectic layers. The alignment is attained by two steps of orientation: A first stress is applied in the isotropic phase in order to orient the mesogens. A second stress forming an angle of 65° with respect to the first stress is exerted in the Sm-X* phase. It forces the smectic layers to be oriented uniformly normal to the *z*-direction (*y*-axis of the sample coordinate system (Figure 2a)). A detailed description of the synthesis of that substance as well as of the orientation procedure is given in refs 3, 4, and 6.

The original sample has a size of 5 × 5 mm^2 (this plane is defined as the *yz*-plane) and a thickness of 500 μm (along the *x*-axis of the sample). To analyze the orientation of the molecular moieties in three dimensions and their static and dynamic behavior under the influence of an external electric field, we have prepared differently aligned sections by micro-

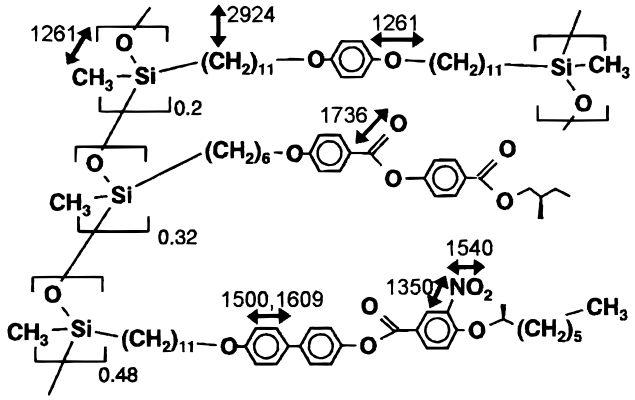

g -13°C Sm-X* 45 Sm-C* 82 Sm-A* 95 is.

Figure 1. Chemical structure and phase transition temperatures of the cross-linkable side chain elastomer. The direction and wavenumbers of the IR transition moments are indicated.

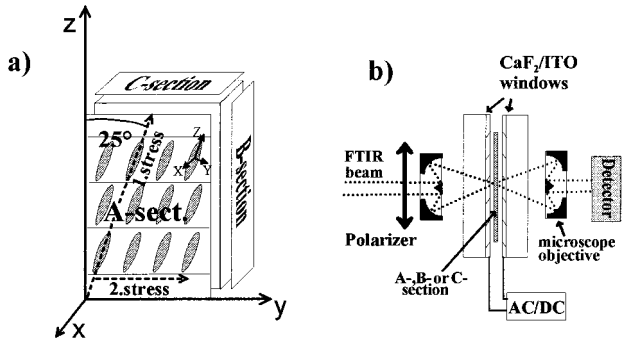

Figure 2. (a) Scheme of the three different microtome-cutted sections. The direction of the two stresses defines the orientation of the mesogen and the smectic layers. Also indicated is the laboratory principal axis frame (L-PAF: *X*, *Y*, *Z*) of the phenyl absorbance. The L-PAF of the other infrared bands differ from this phenyl L-PAF. (b) Experimental setup for the polarized FTIR measurements of microtomized sections under the influence of an external electric field.

* Author for correspondence.
† University of Leipzig.
‡ Inst. Macromolecular Compounds.
§ University of Freiburg.

10.1021/ma981361q CCC: $18.00 © 1999 American Chemical Society
Published on Web 05/06/1999

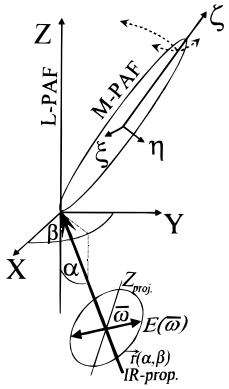

Figure 3. Scheme of the principal axis frames of the molecules (M-PAF: ξ, η, ζ) and of the laboratory system (L-PAF: *X*, *Y*, *Z*) for an individual absorption band. The absorbance ellipsoid in the M-PAF is indicated. The polarized IR beam $\mathbf{r}(\alpha,\beta)$ is used to measure the absorbance ellipsoid in the L-PAF which is connected to the ellipsoid in the M-PAF via the order parameters *S* and *D*. The corresponding fluctuations are indicated by the dotted arrows.

tomizing the sample either in the direction normal to the *x*-, *y*-, or *z*-axis. These 5 μm thick sections are named A-, B-, and C-section, respectively (Figure 2a).

2.2. FTIR Setup. A Bio-Rad Fourier transform infrared (FTIR) spectrometer (FTS 6000) coupled to an IR microscope (UMA 500) with a 100 μm × 100 μm spot has been used to record IR spectra at different polarizations of the IR beam. The microtomized sections were placed between two CaF_2 windows covered with ITO electrodes (Figure 2b). These windows and electrodes are transparent for IR as well as for visible light. The windows were separated by polyimide spacers of 5−8 μm in thickness to avoid electrical short circuits and mechanical stress on the sample. The measurement cell is mounted into a temperature-controlled sample holder (temperature range 20−160 °C, accuracy 0.1 °C). The static absorbance spectra are measured for a set of polarizer directions ω from 0° to 180° with steps of 10°. For a spectrum the wavenumber is recorded from ν = 4000 to 400 cm^{-1}. The absorbance due to an individual band $A_\nu(\omega)$ is determined as the maximum absorbance in the corresponding wavenumber region relative to an appropriate baseline. The absorbance for an IR-active vibration with wavenumber ν depends on the angles between the corresponding transition moments $\mathbf{m}_\nu$ and the electric field vector of the polarized IR beam $\mathbf{E}(\omega)$:

$$A_\nu(\omega) \sim \int (\mathbf{m}_\nu \mathbf{E}(\omega))^2 \, d\tau \tag{1}$$

where the integral is taken over all transition moments in the measurement spot. Equation 1 describes an ellipsoid so that the distribution of these transition moments can be represented by a symmetric second rank tensor. In the frame of an individual molecule (or molecular part, e.g., an individual mesogen or alkyl spacer chain) this second rank tensor $A_{\iota\kappa}$ is only dependent on the conformation of this molecule whereas in the laboratory frame the orientation order must be taken into account as well (Figure 3).

For the description of the anisotropic parts of these absorbance tensors $a_{\iota\kappa} = A_{\iota\kappa} - {}^1/_3 \mathrm{Tr}\{A_{\iota\kappa}\}\delta_{\iota\kappa} = A_{\iota\kappa} - {}^1/_3 A\delta_{\iota\kappa}$, we follow the approach of Schmiedel,[23] who introduced five real components which are for the molecular frame (MF, ξ, η, ζ):

$$W_m^{mol} = (\sqrt{3/2}a_{\zeta\zeta}, \sqrt{1/2}(a_{\xi\xi} - a_{\eta\eta}), \sqrt{2}a_{\xi\eta}, \sqrt{2}a_{\xi\zeta}, \sqrt{2}a_{\eta\zeta}) \tag{2}$$

and for the laboratory frame (LF: *x*, *y*, *z*):

$$W_l^{lab} = (\sqrt{3/2}a_{zz}, \sqrt{1/2}(a_{xx} - a_{yy}), \sqrt{2}a_{xy}, \sqrt{2}a_{xz}, \sqrt{2}a_{yz}) \tag{3}$$

For that a simple relation between the average values of the components in the molecular frame and the laboratory frame is found:

$$\langle W_l^{lab} \rangle = \langle W_m^{mol} S_{ml} \rangle \approx \langle W_m^{mol} \rangle \langle S_{ml} \rangle \tag{4}$$

where in the most general case S_{ml} is a ordering matrix with 25 independent elements that can be described by use of the well-known elements of the Saupe ordering matrix.[23,24]

For the case that the principal axis frame is chosen as molecular frame (M-PAF, Figure 3) the absorbance tensor is described by the diagonal elements $(a_{\xi\xi}, a_{\eta\eta}, a_{\zeta\zeta}) \equiv (a_\xi, a_\eta, a_\zeta) = (m_\xi^2, m_\eta^2, m_\zeta^2)$, so that of the W_m^{mol} components just $W_1^{mol} =$ and $\sqrt{3/2}a_\xi$ and $W_2^{mol} = \sqrt{1/2}(a_\xi - a_\eta)$ remain nonzero. If also for the laboratory system the principal axis frame (L-PAF) of the absorbance ellipsoid (*X*, *Y*, *Z*) is chosen (Figure 3), only $W_1^{lab} = \sqrt{3/2}a_Z$ and $W_2^{lab} = \sqrt{1/2}(a_X - a_Y)$ persist. For an arbitrary infrared propagation vector described in this L-PAF (*X*, *Y*, *Z*) by $\mathbf{r}$ = (sin α cos β, sin α sin β, cos α) the electrical field vector of the IR beam in the L-PAF is

$$\frac{\mathbf{E}(\varpi)}{|\mathbf{E}|} = (-\cos\varpi\cos\alpha\cos\beta - \sin\varpi\sin\beta, \; -\cos\varpi\cos\alpha\sin\beta + \sin\varpi\cos\beta, \cos\varpi\sin\alpha) \tag{5}$$

where ϖ is the angle of the *E*-field vector with respect to the projection of the *Z*-axis onto the plane normal to the beam propagation $\mathbf{r} = \mathbf{r}(\alpha,\beta)$ (Figure 3). In contrast to that, the polarizer angle ω always refers to a sample coordinate axis and $\vartheta_{proj} \equiv (\omega - \varpi)$ is the angle between the projections of the *Z*-axis and the sample axis onto the plane normal to $\mathbf{r}$.

In the L-PAF the polarizer-dependent absorbance is expressed as

$$A(\varpi) = A_X E_X^2/E^2 + A_Y E_Y^2/E^2 + A_Z E_Z^2/E^2 = \frac{1}{3}A + \sqrt{\frac{2}{3}}W_1^{lab}\left(\frac{3}{2}E_Z^2/E^2 - \frac{1}{2}\right) + \sqrt{\frac{1}{2}}W_2^{lab}(E_X^2/E^2 - E_Y^2/E^2) \tag{6}$$

where the relation $E^2 = E_X^2 + E_Y^2 + E_Z^2$ was used and ${}^1/_3 A = {}^1/_3(A_X + A_Y + A_Z)$ denotes the isotropic part of the absorbance.

For the further discussion two cases of the direction of the IR beam are important: propagation in the *YZ*-plane ($\beta = 90°$) and along the *X*-axis ($\alpha = 90°, \beta = 0°$):

$$A(\varpi,\alpha,\beta{=}90°) = \frac{1}{3}A + \sqrt{\frac{2}{3}}W_1^{lab}\left(\frac{3}{2}\sin^2\alpha\cos^2\varpi - \frac{1}{2}\right) + \sqrt{\frac{1}{2}}W_2^{lab}(1 - \cos^2\varpi(1 + \cos^2\alpha)) \tag{7a}$$

$$A(\varpi,\alpha{=}90°,\beta{=}0°) = \frac{1}{3}A + \sqrt{\frac{2}{3}}W_1^{lab}\left(\frac{3}{2}\cos^2\varpi - \frac{1}{2}\right) - \sqrt{\frac{1}{2}}W_2^{lab}\sin^2\varpi \tag{7b}$$

In both equations extremum absorbance ($dA/d\varpi = 0$) is obtained for $\varpi = 0°$, which is equivalent to ($dA/d\omega = 0$) at $\omega_{min,max} = \vartheta_{proj}$.

The parameters S_{11} and S_{21} introduced in eq 4 describe the ordering of the molecular principal axes ξ and of the difference of η and ζ with respect to the laboratory *Z*-axis. S_{11} is the Saupe orientational order parameter *S* and $\sqrt{3}S_{21}$ is the transverse order parameter *D*. With the other order parameters S_{12} and S_{22} the biaxiality of the tilted LC phase is taken into account. In this paper we analyze among other results the transition moments of polar groups and of the phenyl groups. They differ in their absorbance ellipsoids in the LF and in the MF. However, as these groups are all parts of the mesogenic segment, they are subject to the same fluctuations and thus the same order parameters.

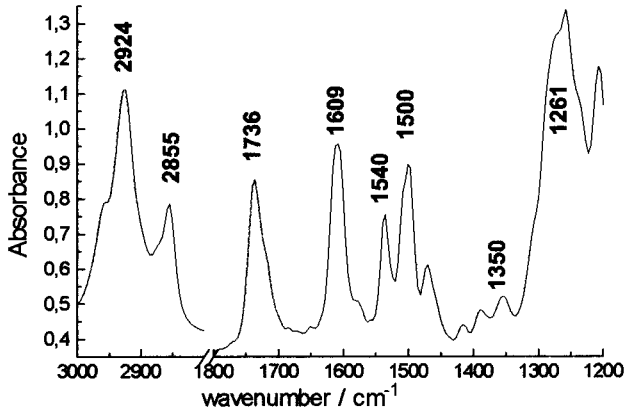

wavenumber /cm^{-1}	assignment:
2924, 2855	ν_{as} (CH_2), ν_s (CH_2); alkyl chains
1736	ν (C=O) carbonyl group of the mesogens
1609, 1500	ν(C-C)$_{aromatic}$; phenylene ring (mesogen & crosslinker)
1540, 1350	ν_{as} (NO_2), ν_s (NO_2) nitro group of the mesogen
1261	δ (Si-CH_3) in the backbone and ν_{as} (C-O-C)

Figure 4. IR absorbance spectrum of the single-crystal FLCE; the wavenumber regime from 2800 to 1800 cm^{-1} is omitted because of graphical reasons.

Equation 6 is derived under some approximations: The relation $E^2_x + E^2_y + E^2_z = E^2 =$ constant is no longer valid if the internal field is taken into account. The (anisotropic) polarizability leads to an additional loss in the intensity of the IR beam so that the absorbance appears larger than calculated by eq 6. Additionally, in an infrared microscope with a short focal length the partial IR beams are inclined to the cell normal which leads to an optical path larger than the cell thickness which also is dependent on the anisotropic optical density.

The spectral resolution was 4 cm^{-1} for the static measurements. A total of 50 scans are co-added for each spectrum, leading to an accuracy of the absorbance of better than 0.01 absorbance units. To obtain a resolution in time of 90 scans/s, the spectral resolution has to be reduced to 16 cm^{-1} for the kinetic measurements. The applied electric field was $\pm 2.6 \times 10^5$V/cm with a frequency of the rectangular pulse of 3 Hz.

3. Results and Discussion

3.1. Assignment of the IR Bands. The IR spectrum of the FLCE and the assignment of selected IR bands used for determination of the orientation of molecular moieties are shown in Figure 4. The CH_2 bands cannot be assigned unequivocally to the flexible spacer chain as there are several other *n*-alkyl chains in the FLCE. The bands assigned to the polysiloxane chain (1261 cm^{-1}) are overlapped by bands due to the C−O−C vibration in the mesogen.

3.2. Molecular Structure of the FLCE in the Different Mesophases. The molecular structure in terms of the absorbance ellipsoids of the different molecular moieties in the LF is derived from the polarizer-dependent absorbance for the A-, B-, and C-section. At first the orientation of the L-PAF of these absorbance ellipsoids with respect to the sample coordinate system is determined. In a further step the absorbance values of these principal axes are estimated.

3.2.1. Average Orientation of the Different Molecular Moieties by Determination of the Corresponding L-PAF. For the A-section in the Sm-C* phase the $A_\nu(\omega)$ plots for the phenyl bands ($\nu = 1500$, 1609 cm^{-1}), the carbonyl band ($\nu = 1736$ cm^{-1}), and the nitro bands ($\nu = 1350$, 1540 cm^{-1}) are presented in Figure 5. The polarizer angle $\omega = 0°$ corresponds to the *z*-axis of the sample, and $\omega = 90°$ corresponds to the *y*-axis. During the whole experiment the principal *X*-axes of all absorbance ellipsoids are equal to the sample *x*-axis (which will be proven in the discussion of the B-section and the C-section). Therefore, in the A-section experiment the principal *Z*-axis and sample *z*-axis are in the plane normal to **r,** and the polarizer angle for which extremum absorbance is obtained ($\omega_{max,min} = \vartheta_{proj}$) directly supplies the angle ϑ between the sample *z*-axis and the principal *Z*-axis (or the *Y*-axis, respectively). The transition moment for the phenyl absorbance forms an angle of approximately 0° to the mesogenic long axis. Its corresponding absorbance ellipsoid in the LF has the director

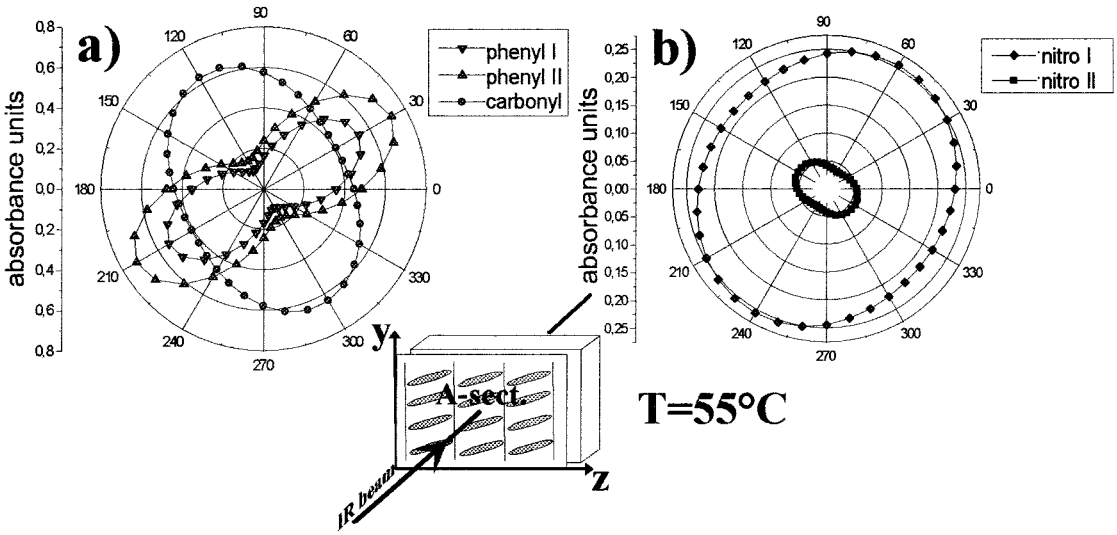

Figure 5. Polar plot of the absorbance vs polarization angle ($A_\nu(\omega)$) for the phenyl-I (1500 cm^{-1}) and the phenyl-II band (1609 cm^{-1}), the carbonyl band (1736 cm^{-1}), the nitro-I (1350 cm^{-1}), and the nitro-II band (1540 cm^{-1}) of the A-section (bookshelf geometry) in the Sm-C* phase (55 °C). The $A_\nu(\omega)$ plots for the carbonyl, the nitro, and the phenyl groups do not have the same symmetry axis which proves the biased rotational distribution of the polar groups around the mesogenic long axis. The experimental error in the absorbance is less than the symbol size.

as principal *Z*-axis and the polarizer angle ω_{max} (phenyl) equals the angle between the director and the sample *z*-axis. In the Sm-C* this angle is ϑ(phenyl) = ω_{max}-(phenyl) = 30° (Figure 5) whereas during the sample orientation process in the Sm-X* this angle has just been 25° (Figure 2a).

In the Sm-C* phase the carbonyl band attains the minimum of absorbance at a polarizer angle of ω_{min}-(carbonyl) = 26° (Figure 5). This deviation of the principal *Z*-axis of the carbonyl absorbance ellipsoid from that of the phenyl absorbance ellipsoid of ω_{max}-(phenyl-I) − ω_{min}(carbonyl) = 4° shows that the mesogenic long axis is not a principal axis of the carbonyl absorbance ellipsoid in the MF. In other words, the carbonyl group has a biased rotational distribution around the mesogenic long axis. The rotational bias of polar groups is the commonly accepted molecular reason for the occurrence of a spontaneous polarization in ferroelectric liquid crystals.[8−10]

The symmetry axes of the $A_\nu(\omega)$ plots of the two nitro bands (Figure 5) are shifted relative to those of the phenyl bands by ω_{max}(phenyl-I) − ω_{min}(nitro-I) = 27°. This shows that also for the nitro group the principal axes for the absorbance ellipsoid in the MF are deviating from the mesogenic long axis. Hence, the rotational distribution of the nitro group is also biased and therefore is a molecular origin of the spontaneous polarization in this FLCE as well.

The $A_\nu(\omega)$ plots of the CH_2 vibration bands and those of the phenyl bands have the same symmetry axis (not shown in the figures). This is in contrast to recent results on FLC polymers where a shift has been observed[10] and is attributed to the "zigzag" arrangements of the mesogen and the spacer. Apparently, this observation is not made in the case of FLCE due to the high amount of CH_2 groups that do not belong to the spacer (i.e., the methylene groups of the cross-linker and the methylene tails of the mesogens that are not connected to the backbone).

The dependence of the director orientation on rising temperature is characterized by an increase of the angle between the director and the *z*-axis (ω_{max}(phenyl-I), Figure 6a). This angle is 25° at room temperature and 37° in the Sm-A phase. This also reflects a change in the orientation of the smectic layers: At room temperature the layer normal is parallel to the *z*-axis (Figure 2a) but inclined by 37° to the *z*-axis in the Sm-A phase (where the layers are normal to the director). A similar movement of the smectic layers was found by temperature-dependent X-ray diffraction on this single-crystal FLCE. To our knowledge this is the first time that a smectic layer movement during phase transitions has been observed in ferroelectric liquid crystals.

As stated above, the biased rotation of the polar groups is reflected by the terms (ω_{min}(nitro-I) − ω_{max}-(phenyl-I)) and (ω_{min}(carbonyl) − ω_{max}(phenyl-I)). For the Sm-C* phase these terms have nonzero values different from those for the Sm-X* phase (Figure 6a). This shows that these two tilted smectic phases can be distinguished by their different rotational distribution functions. In the Sm-A* phase the $A_\nu(\omega)$ plots for all bands have the same symmetry axis (ω_{min}(nitro-I) = (ω_{min}(carbonyl) = ω_{max}(phenyl-I)) = 37 ± 2°). This is the expected behavior since in a nontilted phase the director is a symmetry axis for all segmental distribution functions.

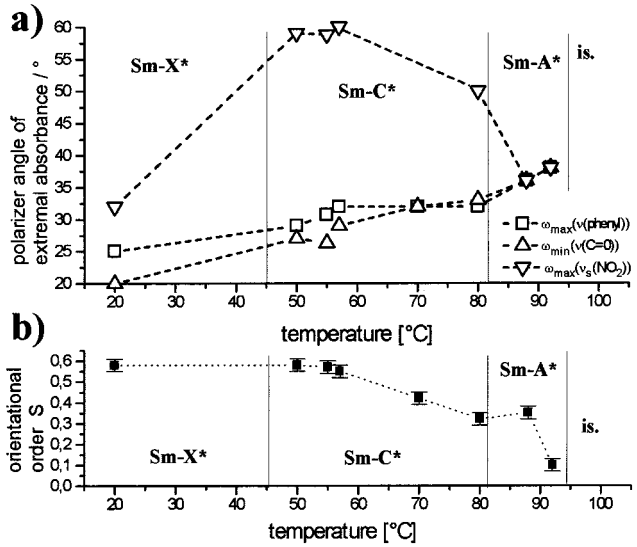

Figure 6. (a) Temperature dependence of the polarizer angle of maximum absorbance for the phenyl-I, the carbonyl, and the nitro-I bands as derived from the different $A_\nu(\omega)$ plots. In the Sm-C* phase a large difference (ω_{max}(phenyl-I) − ω_{min}-(nitro-I)) due to the biased rotational distribution of the nitro group is observed. For T = 70 °C the orientation of the nitro group could not be determined. (b) The temperature dependence of the orientational order parameter *S*. These values are just a lower limit of *S*, and they are calculated from the dichroic ratio of the phenyl-I absorbance.

The absorbance plots $A_\nu(\omega)$ for the C-section (cut parallel to the smectic layers) are characterized by identical symmetry axes ($dA/d\omega = 0$ at $\omega = 0°$ and $\omega = 90°$) for all temperatures and IR absorbance bands (Figure 7). In the C-section experiment the sample *x*-axis is represented by $\omega = 90°$. Hence, this *x*-axis always equals a symmetry axes of the $A_\nu(\omega)$ plots (i.e., the principal *X*-axis of the absorbance ellipsoids).

For the B-section the symmetry axes of all the $A_\nu(\omega)$ absorbance plots are fixed at $\omega \approx 0°$ for all temperatures. This result also shows the equivalence of the principal *X*-axis of all absorbance ellipsoids with the *x*-axis of the sample coordinate system. Summarizing the results, one can state that the orientation of the principal axes of the absorbance ellipsoids in the LF are fully determined by the equivalence of the principal *X*-axis and the sample *x*-axis and by the angles ϑ of the different principal *Z*-axes (with respect to the sample *z*-axis) as determined by the A-section measurements.

3.2.2. Determination of the Values of the Principal Axes of the Absorbance Ellipsoids. Due to the equivalence of the principal *X*-axis and the sample *x*-axis, one can use $A(\varpi, \alpha=90°, \beta=0°)$ of eq 7b to simulate the polarizer-dependent absorbance for the A-section and $A(\varpi, \alpha, \beta=90°)$ of eq 7a for the B- and C-section. The angle α between the IR beam and the *Z*-axes of the different absorbance ellipsoids are $\alpha = \vartheta$ for the C-section measurement and $\alpha = 90° - \vartheta$ for the B-section measurement. (The different ϑ are known from the A-section measurements.) The values for the principal axes of each absorbance ellipsoid ($^1/_3A$), (a_z), ($a_x - a_y$) are determined by fitting eqs 7a and 7b respectively to the experimental $A_\nu(\omega)$ data for the A-, B-, and C-section. Due to experimental errors (e.g., the approximations for the derivation of eq 6), these fitting results are not in full accordance with one another so that only qualitative estimations for the values of the principal

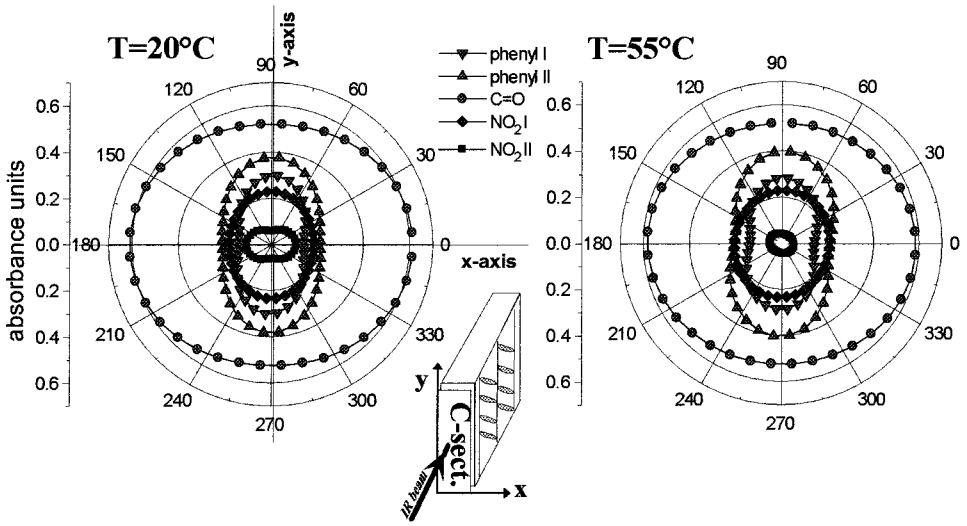

Figure 7. Polar plot of the C-section (homeotropic orientation) in the Sm-X* (20 °C) and the Sm-C* phase (55 °C).

axes of the absorbance ellipsoids can be derived:

$$a_z \gg a_x \quad \text{and} \quad a_x \approx a_y \quad \text{for the phenyl bands} \quad (8a,b)$$

$$a_z < 0 \quad \text{and} \quad a_x < a_y \quad \text{for the carbonyl band} \quad (8c,d)$$

$$a_z > 0 \quad \text{and} \quad a_x < a_y \quad \text{for the nitro-II band} \quad (8e,f)$$

For the absorbance ellipsoid of the nitro-I band deviations between the three principal axes values cannot be derived from the measurements.

3.2.3. Determination of Order Parameters and Rotational Distribution Functions. For the phenyl group the angle between transition moment and mesogenic long axis is known to be approximately 0°. The corresponding absorbance ellipsoid in the molecular principal axis frame (M-PAF) can be simplified to (0,0,*A*) with the mesogenic long axis as ζ-axis. Thus, one obtains from eqs 2−4

$$W_1^{\text{mol}} = \sqrt{\frac{3}{2}}A \quad \text{and} \quad W_2^{\text{mol}} = 0 \qquad (9a,b)$$

which yields

$$\sqrt{\frac{3}{2}}a_Z = W_1^{\text{lab}} = S_{11}\sqrt{\frac{3}{2}}A \quad \text{and}$$

$$\sqrt{\frac{1}{2}}(a_X - a_Y) = W_2^{\text{lab}} = S_{21}\sqrt{\frac{2}{3}}A \quad (9c,d)$$

The estimation $a_x \approx a_y$ (eq 8b, uniaxiality of the phenyl absorbance ellipsoid in the LF) leads to the result that the transverse order parameter $D = \sqrt{3}S_{21}$ is close to zero in this system. Furthermore, the orientational order parameter $S = S_{11}$ can be determined from the A-section measurement according to $S = (R - 1)/(R + 2)$ with R being the "dichroic" ratio of maximal and minimal phenyl absorbance. This lower limit of the order parameter runs from $S_{\text{min}} = 0.58$ down to $S_{\text{min}} = 0.10$ when the sample is heated from room temperature to 92 °C. The small but finite value of S near the phase transition Sm-A*/isotropic shows a broadening of this phase transition which probably is due to inhomogenities of the sample (e.g., inhomogeneously distributed cross-links).

For the polar groups the relation $a_x < a_y$ (eqs 8d and 8f) expresses the biaxiality of the absorbance ellipsoids and leads to

$$0 > W_2^{\text{lab}} = \sqrt{\frac{1}{2}}(a_X - a_Y) = S_{21}W_1^{\text{mol}} + S_{22}W_2^{\text{mol}} = S_{22}\sqrt{\frac{1}{2}}(a_\xi - a_\eta) \quad (10)$$

where $S_{21} = 0$ is known from the analysis of the phenyl absorbance. As $S_{22} > 0$ by definition,[23,24] eq 10 states that for the absorbance ellipsoids in the MF of both polar groups $a_\xi < a_\eta$. The angle between the ζ-axis of the absorbance ellipsoid and the mesogenic long axis equals the angle between the principal *Z*-axis of the L-PAF and the director. In case of the carbonyl group, this angle is 4° (Figures 5 and 6a), which is much less than in other FLC samples.[9−12] This small angle and the fact that we have to take three different carbonyl groups into consideration does not allow an unequivocal quantitative determination of the rotational bias.

For the symmmetric vibration of the nitro band the ζ-axis of the absorbance ellipsoid forms an angle of 27° to the mesogenic long axis. This can be simulated by a totally biased rotation of the nitro group around the mesogenic long axis with a rotational distribution function $f(\psi) = \delta(\psi - \psi_0) + \delta(\psi + \psi_0)$. ψ is the azimuthal angle of the transition moment with respect to the ξ-axis, and the most probable orientation is denoted by $\psi = \psi_0$. With the transition moment forming an angle of approximately 30° to the mesogenic long axis, ψ_0 must be 62° in order to obtain a tilt of the ζ-axis of 27°. Other distribution functions with a weak biasing but with a larger ψ_0 can be also used for the simulation of the measured tilt of the ζ-axis. This result is in accordance with the relation $a_\xi < a_\eta$, which is equivalent to $\psi_0 > 45°$ and which shows that the molecular dipole component in the tilt plane (along the η-axis) is higher than that normal to it (ξ-axis).

3.3. Molecular Orientation in the Static *E*-Field. The switching of the molecules in the microtome cut sections is investigated by applying an external electric field normal to the plane of the microtomized section. For the B-section Figure 8 shows the rotation of the $A_\nu(\omega)$ plot of the phenyl-II band (1609 cm^{-1}) by +15° and −15° respectively for a dc field of $E_{\text{external}} = +2.6 \times 10^5$ and -2.6×10^5 V/cm. These shifts of the $A_\nu(\omega)$ plot are accompanied by an increase of the dichroic ratio from

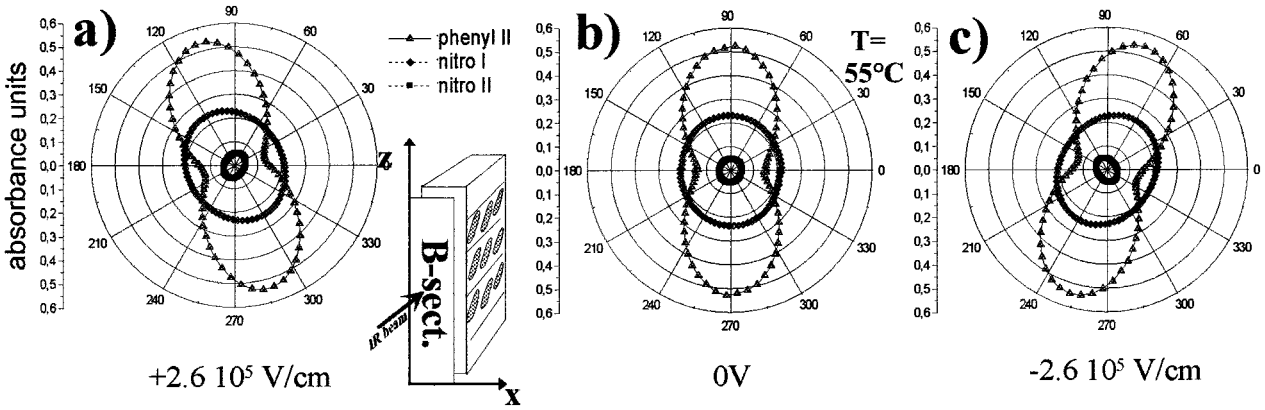

Figure 8. Absorbance vs polarizer angle for the phenyl-II, the nitro-I, and the nitro-II bands at different external electrical fields (in the Sm-C* phase (55 °C) and for the B-section).

3.7 to 4.6. The $A_\nu(\omega)$ plots for the phenyl-I band (1500 cm^{-1}), the carbonyl band, and the methylene band are also rotated by +15° and −15° (not shown here).

The observed switching of the FLCE is different from the bistable ferroelectric switching in surface stabilized cells.[2] The strongly cross-linked SC-FLCE has only one stable state which is defined as the molecular orientation that is fixed by the elastomeric network. The application of the electric field induces a displacement of the mesogens from this state. Since the spontaneous polarization **P** of the FLCE is directed to the normal of the tilting plane (here the *x*-axis) and since for the B-section the applied external electric field is perpendicular to this polarization, the electric field causes a torque $\mathbf{P} \times \mathbf{E}_{\text{external}}$ to the mesogens.

The observed reorientation takes place on a restricted path of a cone which can be derived from Figure 8 (B-section). Analyzing the position of extremum absorbance of the nitro bands ($\omega_{\min}$(nitro-I), $\omega_{\max}$(nitro-II)), one can note a shift of 25° relative to $\omega_{\max}$ of the phenyl bands if an electric field is applied (Figure 8a,c). Without an electric field the extrema of the $A_\nu(\omega)$ plots of all bands are located at the same position (Figure 8b). Because of $\omega_{\max,\min} = \vartheta_{\text{proj}}$, this result reflects that at zero voltage the different principal *Z*-axes are all projected onto the same axis in the plane normal to the beam propagation (i.e., the sample *z*-axis represented by $\omega = 90°$). In an external electric field different ϑ_{proj} values are observed ($\omega_{\max}$(nitro-I) ≠ $\omega_{\max}$(phenyl-I) ≠ $\omega_{\min}$(nitro-II), Figure 8a,c). The different ϑ_{proj} values show that the projections of the different principal *Z*-axes are no longer equal to the sample *z*-axis and therefore that all absorbance ellipsoids (including the director) have rotated on a cone.

Neither in the A-section nor in the C-section can any switching be observed. Especially this result for the A-section is in contrast to un-cross-linked FLC polymers and low molecular mass FLC where in the bookshelf geometry the parallelity of the spontaneous polarization and the external electric field leads to large electrooptical effects. Obviously the forces due to the elastic network are the main reason for the fact that a director reorientation does not take place in the A-section. The observed director reorientation in the B-section experiment by an angle of $\Delta\omega = \omega_{\max}(E_{\text{external}}) - \omega_{\max}(0\ \text{V/cm}) = \pm 15°$ is equivalent to a rotation angle on the cone of

$$\phi_\pm = \arcsin(\tan \Delta\omega \tan \vartheta) = \pm 35° \qquad (11)$$

(with the director tilt $\vartheta = 25°$). In the projection of the A-section such a rotation of the director would have been easily detected. However, the A-section does not show any differences because the electric field leads in the A-section to a much weaker alteration of the Gibbs free energy density than it does in the B-section. This is mainly due to the fact that in the A-section the field-dependent part of the free energy density is $\mathbf{P}\cdot\mathbf{E}_{\text{external}} = PE_{\text{external}} \cos \phi$ whereas in the B-section it is $\mathbf{P}\cdot\mathbf{E}_{\text{external}} = PE_{\text{external}} \sin \phi$. Therefore, in the A-section much higher fields are necessary to compensate for the elastic energy produced by small mesogen elongations in ϕ.

3.4. Time-Resolved FTIR. Time-resolved measurements supply information about the mutual arrangement of molecular parts during the reorientation process. By a detailed comparison of the response of different bands, one can get information about the inter- and intramolecular interaction in that material. In the measurements presented in this report the IR polarizer was held fixed in a position where a maximum of the absorbance modulation for all bands was achieved. The received responses for distinct bands are different concerning the amplitude and direction of these absorbance changes. As in our case the response for only one polarizer angle is recorded; the information on the orientation is reduced from three dimensions to one. Therefore, this kind of data is mainly used to determine the synchronicity in response of the selected bands. To compare the reorientation velocities, the normalized absorbances $A_N(t)$ of corresponding bands were calculated as

$$A_N(t) = (A(t) - A_1)/(A_2 - A_1) \qquad (12)$$

with $A(t)$ being the measured absorbance at time t and A_1 and A_2 being the averaged absorbance for $t = 310-330$ ms and $t = 150-170$ ms, respectively.

The results are presented in Figure 9.

With respect to the signal-to-noise-ratio of the different bands, the normalized absorbance plot in Figure 9b demonstrates a synchronous switching of the investigated bands in the FLCE within a time scale of 10 ms. The switching time of this FLCE is approximately 100 ms under a field of $\pm 2.6 \times 10^5$ V/cm. It should be mentioned that these measurements do not allow to exclude noncooperative motions in a time scale less than 10 ms. Nevertheless, in the case of a FLC dimer and a FLC polymer we could already proof the cooperativity down to the microsecond time scale.[10,12]

4. Conclusion

By means of polarized FTIR spectroscopy, we have investigated the molecular structure of a mechanical

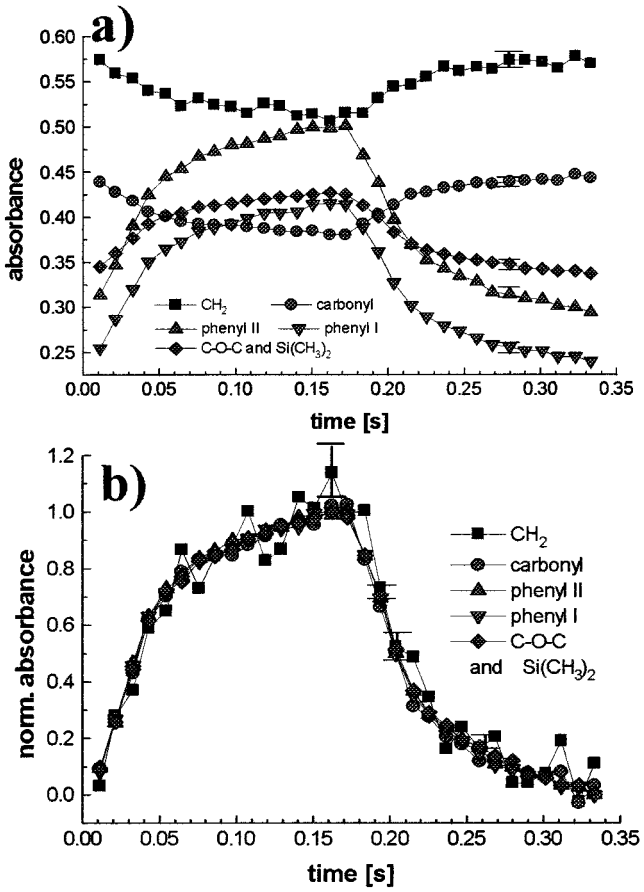

Figure 9. Kinetic measurement of the IR absorbance in the B-section (a) and their normalized absorbance plot (b). The resolution in time is 10 ms. Due to the weaker dichroic ratio of the methylene and the carbonyl band, the errors for their normalized absorbance are larger (±0.1 and ±0.06) than for the other bands (±0.04).

oriented SC-FLCE in its different mesophases and the molecular mobility in response to an external electrical field. For increasing temperatures we measured the decrease of the orientational order parameter from $S =$ 0.58 to 0.1 as well as the changes in the orientations of various molecular moieties. The biased rotational distribution of the carbonyl and the nitro group was analyzed in its dependence on the temperature. It was shown that during heating from the Sm-X* to the Sm-A* phase the smectic layers move to a much larger extent than the mesogens do. The cross-linking of the polymer network in this FLCE restricts the path of the director reorientation in response to an external electric field. The director reorientation takes place on a tilt cone, but the switching is not bistable. The only stable state is the molecular arrangement that was fixed during the cross-linking of the network. Time resolved measurements show that each of the investigated bands is changed during the reorientation process. The amplitude and sign of their response to the electric field is different, but normalization of these responses shows that the corresponding molecular moieties are switching synchronously on a time scale of 10 ms. The switching time is about 100 ms under the influence of a rectangular pulsed electric field of $\pm 2.6 \times 10^5$ V/cm.

Acknowledgment. We thank R. Stannarius for fruitful discussions. Support by the Innovationskolleg "Phänomene an den Miniaturisierungsgrenzen" and the scholarship for S.V.S. by the Alexander-von-Humboldt-Foundation are highly acknowledged.

References and Notes

(1) Gebhard, E.; Brehmer, M.; Zentel, R.; Reibel, J.; Decher, G.; Brodowsky, H. M.; Kremer, F. In *The Wiley Polymer Networks Group Review;* te Nijenhuis, K., Mijs, W., Eds.; John Wiley Sons Ltd.: Chichester, 1997; Vol. 1.
(2) Brehmer, M.; Zentel, R.; Giesselmann, F.; Germer, R.; Zugenmaier, P. *Liq. Cryst.* **1996**, *21***,** 589.
(3) Eckert, T.; Finkelmann, H.; Keck, M.; Lehmann, W.; Kremer, F. *Macromol. Rap. Commun.* **1996**, *17*, 767.
(4) Semmler, K.; Finkelmann, H. *Polym. Adv. Technol.* **1994**, *5*, 231.
(5) Semmler, K.; Finkelmann, H. *Macromol. Chem. Phys.* **1995**, *196*, 3197.
(6) Lehmann, W.; Gattinger, P.; Keck, M.; Kremer, F.; Stein, P.; Eckert, T.; Finkelmann, H. *Ferroelectrics*, in press.
(7) Mauzac, M.; Nguyen, H.-T.; Tournilhac, F.-G.; Yablonsky, S.-V. *Chem. Phys. Lett.* **1995**, *240*, 461.
(8) Schönfeld, A.; Kremer, F. *Ber. Bunsen-Ges. Phys. Chem.* **1993**, *97*, 1237.
(9) Miyachi, K.; Matsushima, J.; Takanishi, Y.; Ishikawa, K.; Takezoe, H.; Fukuda, A. *Phys. Rev. E* **1995**, *52***,** R2153.
(10) Shilov, S. V.; Skupin, H.; Kremer, F.; Gebhart, E.; Zentel, R. *Liq. Cryst.* **1997**, *22***,** 203.
(11) Shilov, S. V.; Skupin, H.; Kremer, F.; Wittig, T.; Zentel, R. *Macromol. Symp.* **1997**, *119*, 261.
(12) Shilov, S. V.; Skupin, H.; Kremer, F.; Wittig, T.; Zentel, R. *Phys. Rev. Lett.* **1997**, *79*, 1686.
(13) Masutani, K.; Yokota, A.; Furukawa, Y.; Tasumi, M.; Yoshizawa, A. *Appl. Spectrosc.* **1993,** *47*, 1370.
(14) Kawasaki, K.; Kidera, H.; Sekiya, T.; Hachiya, S. *Ferroelectrics* **1993**, *148*, 233.
(15) Shilov, S. V.; Okretic, S.; Siesler, H. W.; Zentel, R.; Öge, T. *Macromol. Chem. Rap. Commun.* **1995**, *16*, 125.
(16) Katayama, N.; Sato, T.; Ozaki, Y.; Murashiro, K.; Kikuchi, M.; Saito, S.; Demus, D.; Yuzawa, T.; Hamaguchi, H. *Appl. Spectrosc.* **1995**, *49*, 977.
(17) Kocot, A.; Kruk, G.; Wrzalik, R.; Vij, J. K. *Liq. Cryst.* **1992**, *12*, 1005.
(18) Zeks, B. *Ferroelectrics* **1984**, *53***,** 33.
(19) Guenzler, H.; Heise, H. M. *IR-Spektroskopie;* vch-Verlag: Weinheim, 1996.
(20) Hide, F.; Clark, N. A.; Nito, K.; Yasuda, A.; Walba, D. M. *Phys. Rev. Lett.* **1995**, *75*, 2344.
(21) Brodowsky, H. M.; Boehnke, U.-C.; Kremer, F.; Gebhard, E.; Zentel, R. *Langmuir* **1997**, *13*, 5378.
(22) Pohl, L. In *Liquid Crystals;* Stegemeyer, H., Guest Ed.; Steinkopff: Darmstadt, 1994.
(23) Schmiedel, H. *Wiss. Z. Karl-Marx-University Leipzig, Math.-Naturwiss. R.* **1984**, *337* (4), 441.
(24) Limmer, St. *Fortschr. Phys.* **1989**, *37* (12), 879.

MA981361Q